New capillary number definition for displacement of residual nonwetting phase in natural fractures

AlQuaimi, B. I.; Rossen, W. R.

DOI
10.1002/2017GL073211

Publication date
2017

Document Version
Final published version

Published in
Geophysical Research Letters

AGU PUBLICATIONS

Geophysical Research Letters

RESEARCH LETTER
10.1002/2017GL073211

Key Points:
- A new definition of capillary number for fractures was defined from a force balance on a trapped ganglion in a fracture
- Three geometric parameters were identified to describe the geometry of the fracture wall surface; these parameters can be determined from analysis of a map of fracture aperture, with no two-phase flow data
- The new definition of capillary number was tested, and the experimental data showed its suitability to describe the flow of nonwetting phase in fractures

Correspondence to:
B. I. AlQuaimi,
b.alquaimi@tudelft.nl

Citation:
AlQuaimi, B. I., and W. R. Rossen (2017), New capillary number definition for displacement of residual nonwetting phase in natural fractures, *Geophys. Res. Lett.*, *44*, 5368–5373, doi:10.1002/2017GL073211.

Received 22 FEB 2017
Accepted 17 MAY 2017
Accepted article online 22 MAY 2017
Published online 3 JUN 2017

New capillary number definition for displacement of residual nonwetting phase in natural fractures

B. I. AlQuaimi[1,2] and W. R. Rossen[1]

[1]Department of Geoscience and Engineering, Delft University of Technology, Delft, Netherlands, [2]Saudi Aramco, Dhahran, Saudi Arabia

Abstract We propose a new capillary number for flow in fractures starting with a force balance on a trapped ganglion in a fracture. The new definition is validated with laboratory experiments using five distinctive model fractures. Capillary desaturation curves were generated experimentally using water-air forced imbibition. The residual saturation-capillary number relationship obtained from different fractures, which vary in aperture and roughness, can be represented approximately by a single curve in terms of the new definition of the capillary number. They do not fit a single trend using the conventional definition of the capillary number.

1. Introduction

Naturally fractured reservoirs (NFRs) have been explored and exploited globally for geothermal energy, petroleum production, coalbed methane production, and nuclear waste sequestration [*Ramspott et al.*, 1979; *Pruess and Tsang*, 1990; *Persoff and Pruess*, 1995]. Understanding and predicting the behavior of NFRs requires understanding the flow in a single fracture [*Rossen and Kumar*, 1992]. A single fracture has rough walls and variable aperture, as well as asperities where the two opposing fracture walls are in contact with each other [*Olsson and Barton*, 2001]. Thus, it can be represented as a two-dimensional network of locations of wide and narrow aperture [*Tsang*, 1984; *Brown and Scholz*, 1985; *Wang and Narasimhan*, 1985; *Brown et al.*, 1986; *Schrauf and Evans*, 1986; *Pyrak-Nolte et al.*, 1988; *Morrow et al.*, 1990; *Rossen and Kumar*, 1992; *Odling and Roden*, 1997; *Hughes and Blunt*, 2001]. Therefore, fractures can be considered as 2-D analogs of the 3-D networks of throats and bodies that compose the pore network of rock matrix [*Rossen and Kumar*, 1992; *Hughes and Blunt*, 2001]. During two-phase flow in a fracture, there is a similar competition between viscous and capillary forces as in rock matrix, which can be represented by a capillary number. However, the capillary number for rock is not adequate to describe the mobilization of nonwetting phase in fractures. *Moore and Slobod* [1955] defined the capillary number N_{ca} as

$$N_{ca} \equiv \frac{V\mu}{\gamma \cos\theta} \tag{1}$$

where V is the superficial velocity, μ is the viscosity of the displacing fluid, γ is the interfacial tension, and θ is the contact angle. Another form of the capillary number uses the permeability of the matrix [*Reed and Healy*, 1977]:

$$N_{ca} \equiv \frac{K|\nabla P|}{\gamma \cos\theta} \tag{2}$$

where K is permeability, $|\nabla P|$ is the magnitude of the pressure gradient, θ is the contact angle, and γ is interfacial tension. One can derive equation (2) from a force balance on a trapped nonwetting ganglion, assuming that pore-throat radius and pore length each scale with the square root of permeability [*Sheng*, 2010]. This assumption is reasonable for geometrically similar porous media like packings of beads or sand. *Hughes and Blunt* [2001] analyzed multiphase flow in a single fracture using a pore-network model. They generated a model of the fracture from published aperture data and defined the capillary number for this model as

$$N_{ca} \equiv \frac{Q\mu_w}{\bar{d}bN_y\gamma} \tag{3}$$

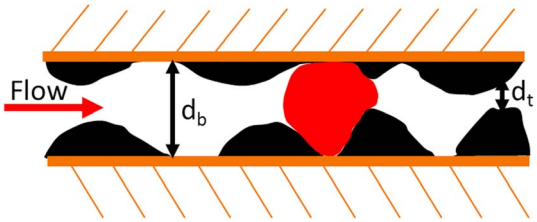

Figure 1. Schematic of rough fracture with a trapped ganglion. The aperture of the fracture is greatly exaggerated in this figure compared to distance along the fracture plane.

where Q is the volumetric flow rate, μ_w is the displacing fluid viscosity (water in this case), $\overline{d}$ is the mean aperture, b is the resolution (width of the pixels), N_y is the number of pixels perpendicular to flow across the fracture, and γ is the interfacial tension. (We have changed their nomenclature for consistency with our derivation below.) This definition is equivalent to equation (1); superficial (Darcy) velocity is replaced by the volumetric flow rate Q divided by cross-sectional area ($\overline{d}bN_y$). The assumption in the derivation of the capillary number for rock from a force balance on a trapped ganglion is that permeability scales with the product of pore-throat radius and pore-body length. This assumption is questionable for fractures, where fracture permeability could be the same for a slit with smooth walls and no trapping and a fracture with large variations in aperture and significant trapping.

2. New Capillary Number Derivation

We present a derivation of the capillary number for a fracture based on force balance on a trapped nonwetting ganglion. The variation of aperture d is the geometric parameter that is responsible for trapping nonwetting phase in the fracture. Capillary pressure across a curved interface where the aperture is d is

$$P_c = \frac{2\gamma \cos\theta}{d} \tag{4}$$

We assume that the length scale along which aperture varies in the fracture plane is much greater than the aperture itself; thus, interfaces are nearly cylindrical rather than spherical. We provide justification below. The principle radii of curvature of the interface between perfectly wetting and nonwetting phases are thus $r_1 = d\cos\theta/2$ and $r_2 \cong \infty$ [*Pruess and Tsang*, 1990]. Consider a fracture with some degree of roughness, where a trapped ganglion is on the verge of forward displacement as shown in the schematic of Figure 1.

The curvature across the fracture is much greater than that within the fracture plane; therefore, the maximum capillary pressure during passage through the throat can be written as

$$P_c = \frac{2\gamma \cos\theta}{d_t} \tag{5}$$

where d_t is the minimum aperture, i.e., aperture at the throat. The capillary pressure difference across the ganglion, with its leading edge penetrating a throat and its trailing edge in a pore body where the aperture is d_b, is given by

$$\Delta P_c = \left(\frac{2\gamma}{d_t} - \frac{2\gamma}{d_b}\right)\cos\theta \tag{6}$$

[*van Golf-Racht*, 1982]. The pressure difference across the ganglion, of length L_g, must be greater than this pressure difference if the ganglion is to be mobilized:

$$\nabla P L_g > \left(\frac{2\gamma}{d_t} - \frac{2\gamma}{d_b}\right)\cos\theta = \frac{2\gamma}{d_t}\left(1 - \left(\frac{d_t}{d_b}\right)\right)\cos\theta \tag{7}$$

One can regroup terms in equation (7) to restate the criterion for mobilization in terms of a dimensionless capillary number:

$$\frac{\nabla P L_g d_t}{2\gamma\left(1 - \left(\frac{d_t}{d_b}\right)\right)\cos\theta} \equiv N_{ca} > 1 \tag{8}$$

Table 1. A Summary of the Geometric Parameters of the Model Fractures (All Values in μm)

	d_H	d_z	d_b	d_t	L_P	L_{cor}
Sample 1	660	0	1118	808	2661	2754
Sample 2	79	8	138	68	819	795
Sample 3	324	54	847	437	5156	4800
Sample 4	116	45	255	145	4415	5100
Sample 5	102	0	198	118	2421	2240

The permeability of a fracture, approximated as a smooth rectangular slit, can also be written as a function of the average hydraulic aperture d_H [*van Golf-Racht*, 1982; *Tsang*, 1992; *Zimmerman and Bodvarsson*, 1996]:

$$k_f = \frac{{d_H}^2}{12} \tag{9}$$

Equation (9) is in effect a definition of the hydraulic aperture d_H. Introducing permeability k_f into equation (8), and noting its relation to d_H, yields

$$\frac{L_g d_t}{1-\left(\frac{d_t}{d_b}\right)\cos\theta} = (d_H)^2\left(\frac{d_t}{d_H}\right)\left(\frac{L_g}{d_t}\right)\left(\frac{d_t}{d_H}\right)\frac{1}{1-\left(\frac{d_t}{d_b}\right)\cos\theta} \tag{10}$$

$$N_{ca} = \left(\frac{\nabla P k_f}{\gamma\cos\theta}\right)\left[\left(\frac{12}{2}\right)\left(\frac{d_t}{d_H}\right)^2\left(\frac{L_g}{d_t}\right)\frac{1}{1-\left(\frac{d_t}{d_b}\right)}\right] \tag{11}$$

The first part of this definition of the capillary number is identical to equation (2), i.e., that traditionally used for porous media. The second part is a geometric term that accounts for the effect of fracture roughness: the narrowness of the "throats," the distance between throats, and the contrast in aperture between pore throats and bodies. A similar geometric term based on the length of a ganglion in the definition of N_{ca} for rock matrix was recently identified [*Yeganeh et al.*, 2016]. To be useful, the terms in this definition must be derivable from a consideration of the fracture itself, without, for instance, needing to conduct a two-phase flow experiment.

We first consider a 2-D network representation of the fracture. We take the characteristic pore-throat aperture d_t to be the aperture at the percolation threshold of this network. We take d_b to be the average pore-body aperture, and the typical length of a pore (L_p) to be L_g. A simpler approach, and equally accurate, we find, is to take the correlation length (L_{cor}) of the aperture distribution for L_p (Table 1). Individual ganglia may differ in length from L_p or L_{cor}, but on average, they are expected to scale with either measure, as in 3-D porous media [*Larson et al.*, 1981; *Chatzis et al.*, 1983; *Mayer and Miller*, 1992]. The value of d_H is determined from the permeability of the fracture, measured in a single-phase flow experiment. In principle it could be derived from flow simulations using the measured aperture distribution. We show below that all the terms can be estimated from a map of aperture or a model for the fracture. Numerous studies characterizing aperture variation and fracture wall roughness could be used to generate such a representation [*Tsang*, 1984; *Brown and Scholz*, 1985; *Wang and Narasimhan*, 1985; *Brown et al.*, 1986; *Schrauf and Evans*, 1986; *Pyrak-Nolte et al.*, 1988; *Morrow et al.*, 1990; *Johns et al.*, 1993; *Hakami and Larsson*, 1996; *Odling and Roden*, 1997; *Oron and Berkowitz*, 1998; *Hughes and Blunt*, 2001; *Karpyn et al.*, 2007; *Lang et al.*, 2015, 2016].

3. Experimental Procedure and Results

We tested this capillary number experimentally as follows. We designed five model fractures made of glass plates: a clear, flat glass plate on the top and rough glass plate on the bottom, glued together at the edges using glass-adhesive material. The plates are also clamped to prevent deformation. Glass plates have been used previously to study flow in fractures [*Wan et al.*, 2000; *Chen et al.*, 2004a, 2004b; *Yan et al.*, 2006; *Speyer et al.*, 2007]. The model fracture is 30 × 10 cm and the area of interest, where the pressure is measured, 16 × 10 cm. As shown below (Table 1), these model fractures exhibit a range of apertures and scales of roughness. The model fracture is placed in a light-isolation box, and light is allowed only from a compact backlight,

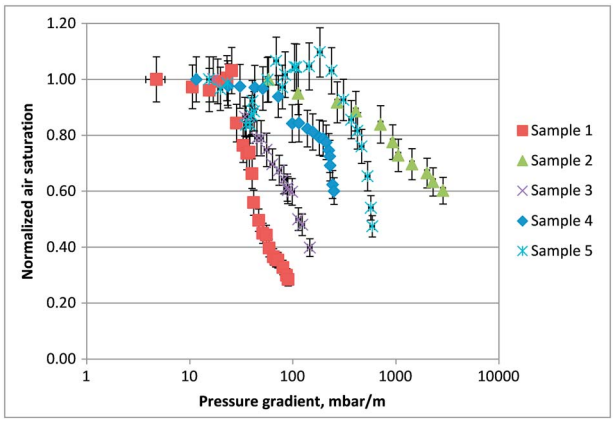

Figure 2. Normalized air saturation in experiments versus pressure gradient for the different five model fractures. The estimated error in the *y* axis represents the uncertainty in the analysis of images of trapped air, while estimated error in the *x* axis represents the maximum error of the pressure sensor.

which provides a constant and even illumination beneath the fracture. A high-definition camera is placed on top of the fracture to capture images during the experiments. Water is injected through a standard infusion pump. The experiments start by measuring the hydraulic aperture of each model fracture by fully saturating the fracture with water, incrementally increasing injection rate, and recording pressure. The rate-pressure relationship was used to estimate the hydraulic aperture is [*Witherspoon et al.*, 1980; *Hakami and Larsson*, 1996]

$$Q = \frac{1}{12}\frac{|\nabla P| w d_H^{\,3}}{\mu} \tag{12}$$

where Q is volumetric flow rate, $|\nabla P|$ is pressure gradient, w is the width perpendicular to flow, d_H is the hydraulic aperture, and μ is the viscosity. The flow experiments for our model fractures showed a linear relationship between Q and $|\nabla P|$, which indicates that the inertial forces were negligible and there was no change in aperture during flow. Table 1, column 1, illustrates the values of the hydraulic aperture.

The hydraulic aperture values and the distribution of the height values were used with the effective medium approximation (EMA) to estimate the gap distance (d_z) between the highest point of the rough plate and the flat top plate. If d_z is zero, then the two plates are estimated to be in contact at the peaks of the roughened plate. It was estimated by comparing the hydraulic aperture from the experiments to that estimated using EMA and aperture distribution:

$$\int_0^\infty n(d)\frac{g_m - g(d)}{g(d) - \left(\frac{Z}{2} - 1\right)g_m}\mathrm{d}d = 0 \tag{13}$$

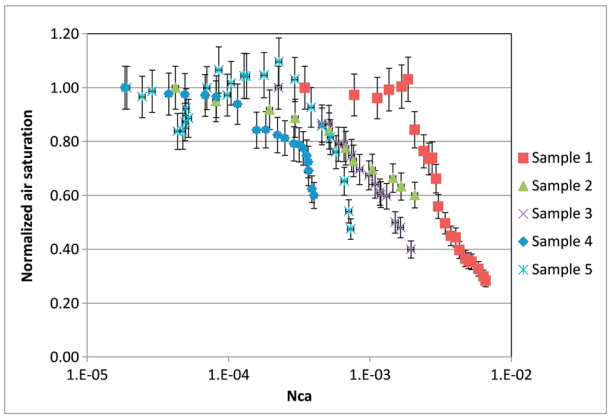

Figure 3. Normalized air saturation in experiments versus conventional capillary number (equation (2)). The trend varies considerably between samples. The plot shows that the trend cannot be captured by the conventional capillary number.

where $n(d)$ is the area fraction of each aperture value, $g(d)$ is the conductivity (d^3) at a location with aperture d, Z is the coordination number of the network, and g_m is the effective conductivity of the medium, i.e., $d_H^{\,3}$. The coordination number Z was selected to be 4 [*Kirkpatrick*, 1973; *Rossen and Kumar*, 1992]. The distance d_z was adjusted until equation (13) was satisfied with $g_m = d_H^{\,3}$. Table 1, column 2, shows the estimated gap d_z between peaks of the rough plate and the top plate in each model fracture. Table 1 also shows that the ratio (d_t/L_p) ranges from about 3 (Sample 1) to about 30 (Sample 4). The width of a throat in

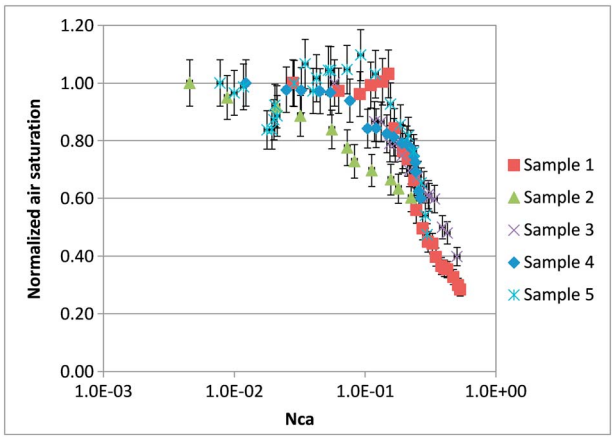

Figure 4. Normalized air saturation in experiments versus new capillary number (equation (11)). The relationship can be represented by approximately a single curve if the defined fracture geometric parameters are considered.

the fracture plane scales with (but is somewhat smaller than) L_p; this indicates that for all the fractures except for Sample 1 our assumption in equation (6) that interface curvature across the fracture aperture is much greater than that within the fracture plane is very good.

Water-air forced imbibition experiments were conducted using dyed (Methylene Blue, 0.001 weight %) water to enhance the contrast between air and water. The fundamental difference between water-air and water-oil imbibition is the surface tension. We assume $\cos\theta = 1$ (perfectly wetting by water), but at any case, it is constant throughout the experiments. In these experiments, the procedure is as follows. The model fracture parts are thoroughly cleaned using ethanol before fabrication. The injected water is demineralized to avoid mineral precipitation. The syringe and tubes are changed for each model fracture experiment. The water is injected at a rate of 0.5 ml/min in horizontal flow, until no further change in residual air saturation is observed. The water-injection rate is increased, and an image is taken when two conditions are satisfied: first, no further change in air saturation is observed, and, second, the pressure is stable for at least 15 min. Successive images are taken with incremental increases in injection rate until a low residual saturation is achieved. The images are loaded into the image-processing software ImageJ to determine the saturation at each pressure gradient. Traditionally, area fraction is used as an approximation to fracture saturation [*Pieters and Graves*, 1994; *Chen et al*., 2004a, 2004b]. We developed two procedures for the analysis of the images: image thresholding to detect the boundary of the ganglion and the built-in finding-edges option in ImageJ. The difference between these two procedures is used as estimated error in the analysis of the saturation (Figure 2, *y* axis). The estimated error in N_{ca} (Figure 2, *x* axis) reflects fluctuations in the measurements of the pressure sensor. Figure 2 shows the relation between air saturation normalized to initial saturation and pressure gradient. In a few cases at relatively low-pressure difference, gas-trapped upstream was displaced into the region we monitored and became trapped there; thus, in a few cases normalized saturation increases before it declines with increasing pressure gradient.

The pressure gradient $|\nabla P|$ required to mobilize ganglia and the rate of change of saturation differ among samples. Figure 3 shows the capillary desaturation curve of the five samples using the conventional capillary number (equation (2)), which is conventionally plotted in a semi-log scale [*Larson et al*., 1981; *Lake et al*., 1986; *Sheng*, 2010]. The scatter is less than in Figure 2, but still, the trend varies by an order of magnitude in N_{ca}. On the other hand, if we use the experimental data along with the geometric parameters we determined for the individual model fractures (equation (11)), namely, d_t, d_b, and L_p, the relationship can be represented by approximately a single curve (Figure 4). The trends for four samples overlie each other, and sample 2 differs from the others by much less than an order of magnitude. The new definition derived from a force balance on a ganglion trapped in a fracture better represents the mobilization of nonwetting discontinuous phase in the fracture, by using the geometric parameters determined for the fracture. As noted, means exist to measure these parameters. Alternatively, it may be possible to develop heuristics to relate fractures of different types (shear or open fractures) or in different geological formations to these parameters, much as N_{ca} correlations in rock are adjusted for different formations [*Larson et al*., 1981; *Lake et al*., 1986].

Acknowledgments
The authors acknowledge Saudi Aramco for providing the scholarship for AlQuaimi to do his PhD and also the generous support provided by the sponsors of the Joint Industry Project on Foam for Enhanced Oil Recovery at Delft University of Technology. Additional data are made available through Delft University of Technology Repository via http://dx.doi.org/10.4121/uuid:b959da2e-f955-4991-b2bc-b2514397671f.

References

Brown, S. R., and C. H. Scholz (1985), Broad bandwidth study of the topography of natural rock surfaces, *J. Geophys. Res.*, *90*(B14), 12575–12582.
Brown, S. R., R. L. Kranz, and B. P. Bonner (1986), Correlation between the surfaces of natural rock joints, *Geophys. Res. Lett.*, *13*(13), 1430–1433.

Chatzis, I., N. R. Morrow, and H. T. Lim (1983), Magnitude and detailed structure of residual oil saturation, *Soc. Pet. Eng. J.*, *23*, 311–326, doi:10.2118/10681-PA.
Chen, C.-Y., K. Li, and R. N. Horne (2004a), *Experimental Study of Phase Transformation Effects on Relative Permeabilities in Fractures*, paper presented at the SPE Annual Technical Conference and Exhibition, Houston, Tex.
Chen, C. Y., R. N. Horne, and M. Fourar (2004b), Experimental study of liquid-gas flow structure effects on relative permeabilities in a fracture, *Water Resour. Res.*, *40*, W08301, doi:10.1029/2004WR003026.
Hakami, E., and E. Larsson (1996), Aperture measurements and flow experiments on a single natural fracture, paper presented at the International Journal of Rock Mechanics and Mining Sciences & Geomechanics Abstracts.
Hughes, R. G., and M. J. Blunt (2001), Network modeling of multiphase flow in fractures, *Adv. Water Res.*, *24*(3–4), 409–421, doi:10.1016/S0309-1708(00)00064-6.
Johns, R. A., J. S. Steude, L. M. Castanier, and P. V. Roberts (1993), Nondestructive measurements of fracture aperture in crystalline rock cores using X ray computed tomography, *J. Geophys. Res.*, *98*(B2), 1889–1900.
Karpyn, Z., A. Grader, and P. Halleck (2007), Visualization of fluid occupancy in a rough fracture using micro-tomography, *J. Colloid Interface Sci.*, *307*(1), 181–187.
Kirkpatrick, S. (1973), Percolation and conduction, *Rev. Mod. Phys.*, *45*(4), 574.
Lake, L. W., R. Johns, W. Rossen, and G. Pope (1986), *Fundamentals of Enhanced Oil Recovery*, pp. 83–88, Society of Petroleum Engineers, Richardson, Tex.
Lang, P., A. Paluszny, and R. Zimmerman (2015), Hydraulic sealing due to pressure solution contact zone growth in siliciclastic rock fractures, *J. Geophys. Res.: Solid Earth*, *120*, 4080–4101, doi:10.1002/2015JB011968.
Lang, P. S., A. Paluszny, and R. W. Zimmerman (2016), Evolution of fracture normal stiffness due to pressure dissolution and precipitation, *Int. J. Rock Mech. Min. Sci.*, *88*, 12–22.
Larson, R. G., H. T. Davis, and L. E. Scriven (1981), Displacement of residual nonwetting fluid from porous media, *Chem. Eng. Sci.*, *36*(1), 75–85, doi:10.1016/0009-2509(81)80049-8.
Mayer, A. S., and C. T. Miller (1992), The influence of porous medium characteristics and measurement scale on pore-scale distributions of residual nonaqueous-phase liquids, *J. Contam. Hydrol.*, *11*(3), 189–213, doi:10.1016/0169-7722(92)90017-9.
Moore, T., and R. Slobod (1955), Displacement of oil by water-effect of wettability, rate, and viscosity on recovery, paper presented at the Fall Meeting of the Petroleum Branch of AIME, Orleans, La.
Morrow, N. R., K. R. Brower, S. Ma, and J. S. Buckley (1990), Fluid flow in healed tectonic fractures, *J. Pet. Technol.*, *42*(10), 1,310–1,318.
Odling, N. E., and J. E. Roden (1997), Contaminant transport in fractured rocks with significant matrix permeability, using natural fracture geometries, *J. Contam. Hydrol.*, *27*(3), 263–283.
Olsson, R., and N. Barton (2001), An improved model for hydromechanical coupling during shearing of rock joints, *Int. J. Rock Mech. Min. Sci.*, *38*(3), 317–329.
Oron, A. P., and B. Berkowitz (1998), Flow in rock fractures: The local cubic law assumption reexamined, *Water Resour. Res.*, *34*(11), 2811–2825.
Persoff, P., and K. Pruess (1995), Two-phase flow visualization and relative permeability measurement in natural rough-walled rock fractures, *Water Resour. Res.*, *31*(5), 1175–1186.
Pieters, D., and R. Graves (1994), Fracture relative permeability: Linear or non-linear function of saturation. paper presented at the International Petroleum Conference and Exhibition of Mexico.
Pruess, K., and Y. W. Tsang (1990), On two-phase relative permeability and capillary pressure of rough-walled rock fractures, *Water Resour. Res.*, *26*(9), 1915–1926, doi:10.1029/WR026i009p01915.
Pyrak-Nolte, L. J., N. G. Cook, and D. D. Nolte (1988), Fluid percolation through single fractures, *Geophys. Res. Lett.*, *15*(11), 1247–1250.
Ramspott, L. D., L. B. Ballou, R. C. Carlson, D. N. Montan, T. R. Butkovich, J. E. Duncan, W. C. Patrick, D. G. Wilder, W. G. Brough, and M. C. Mayr (1979), Technical concept for test of geologic storage of spent reactor fuel in the climax granite, Nevada Test Site (UCID--18197; TRN: 79:015546 United StatesTRN: 79:015546Mon Feb 04 15:44:52 EST 2008NTIS, PC A04/MF A01LLNL; SCA: 050900; PA: ERA-04:045988; EDB-79:092686; NNS-85:000189; SN: 85000189English).
Reed, R. L., and R. N. Healy (1977), Some physicochemical aspects of microemulsion flooding: A review, *Improved Oil Recovery by Surfactant and Polymer Flooding*, 383–437, https://doi.org/10.1016/B978-0-12-641750-0.50017-7.
Rossen, W., and A. T. Kumar (1992), Single-and two-phase flow in natural fractures, paper presented at the SPE Annual Technical Conference and Exhibition, Washington, D. C.
Schrauf, T., and D. Evans (1986), Laboratory studies of gas flow through a single natural fracture, *Water Resour. Res.*, *22*(7), 1038–1050.
Sheng, J. (2010), *Modern Chemical Enhanced oil Recovery: Theory and Practice*, pp. 293–297, Gulf Professional, Burlington, Mass.
Speyer, N., K. Li, and R. Horne (2007), Experimental measurement of two-phase relative permeability in vertical fractures, paper presented at the Proceedings, Thirty-Second Workshop on Geothermal Reservoir Engineering Stanford Univ., Stanford, Calif.
Tsang, Y. (1984), The effect of tortuosity on fluid flow through a single fracture, *Water Resour. Res.*, *20*(9), 1209–1215.
Tsang, Y. (1992), Usage of "equivalent apertures" for rock fractures as derived from hydraulic and tracer tests, *Water Resour. Res.*, *28*(5), 1451–1455.
van Golf-Racht, T. D. (1982), *Fundamentals of Fractured Reservoir Engineering*, vol. 12, pp. 147–157, Elsevier, Amsterdam, Netherlands.
Wang, J., and T. N. Narasimhan (1985), Hydrologic mechanisms governing fluid flow in a partially saturated, fractured, porous medium, *Water Resour. Res.*, *21*(12), 1861–1874.
Wan, J., T. K. Tokunaga, T. R. Orr, J. O'Neill, and R. W. Connors (2000), Glass casts of rock fracture surfaces: A new tool for studying flow and transport, *Water Resour. Res.*, *36*(1), 355–360.
Witherspoon, P. A., J. S. Wang, K. Iwai, and J. E. Gale (1980), Validity of cubic law for fluid flow in a deformable rock fracture, *Water Resour. Res.*, *16*(6), 1016–1024.
Yan, W., C. A. Miller, and G. J. Hirasaki (2006), Foam sweep in fractures for enhanced oil recovery, *Colloids Surf., A*, *282*, 348–359.
Yeganeh, M., J. Hegner, E. Lewandowski, A. Mohan, L. W. Lake, D. Cherney, A. Jusufi, and A. Jaishankar (2016), Capillary desaturation curve fundamentals, paper presented at the SPE Improved Oil Recovery Conference, Okla.
Zimmerman, R. W., and G. S. Bodvarsson (1996), Hydraulic conductivity of rock fractures, *Transp. Porous Media*, *23*(1), 1–30.